# Direct numerical simulations and models for hot burnt gases jet ignition

Quentin Malé, Olivier Vermorel, Frédéric Ravet, Thierry Poinsot

# Direct Numerical Simulations and Models for Hot Burnt Gases Jet Ignition

Quentin Malé[a,b,*], Olivier Vermorel[a], Frédéric Ravet[b], Thierry Poinsot[a,c]

[a] *CERFACS, 42 Avenue Gaspard Coriolis, 31057 Toulouse Cedex 01, France*
[b] *Renault SAS, 1 Avenue du Golf, 78288 Guyancourt Cedex, France*
[c] *CNRS, IMFT, 1 Allée du Professeur Camille Soula, 31400 Toulouse Cedex, France*

**Abstract**

This is a pre-print of an article accepted for publication in:

**Combustion and Flame**.

The final authenticated version is available online at:

`https://doi.org/10.1016/j.combustflame.2020.09.017`

This work uses multiple three-dimensional Direct Numerical Simulations (DNSs) to i) investigate the ignition process of a cold lean premixed mixture at atmospheric conditions by a jet of hot burnt gases that may be cooled before injection ii) evaluate models able to predict the outcome of such a scenario in terms of ignition. Understanding and being able to model ignition of cold premixed mixtures by hot burnt gases is essential to design systems like engines (to ensure ignition) and flameproof enclosures (to prevent ignition). Limited work has focused on the combined effects of the jet injection speed and temperature on ignition. This is difficult to do by using experiments only and DNS is a natural approach to gain knowledge on that point. By varying the hot jet injection speed and temperature, the three-dimensional, kinetically detailed, DNSs allow a parametric study of the impact of these parameters on the ignition process and provide data to build and test models. Simulations prove that jet injection speed and temperature (usually less than the adiabatic flame temperature because of cooling effects through the injection hole) directly govern ignition.

*Corresponding author
*Email address:* `male@cerfacs.fr` (Quentin Malé)

Chemical Explosive Mode Analysis (CEMA) is used to characterize the reacting flow structure which is strongly impacted by the jet injection speed. Based on the DNSs conclusions, a zero-dimensional Lagrangian model where a small element of the jet burnt gases mixes at a certain rate with the fresh gases while it potentially ignites is found to be a good candidate to predict the outcome of an ignition sequence (success or failure).

*Keywords:* turbulent jet ignition, pre-chamber ignition, internal combustion engine, flameproof enclosure

## 1. Introduction

The process of ignition of cold streams by jets of hot burnt gases is critical in many applications including flameproof enclosures [1, 2], reciprocating engines [3, 4, 5], wave rotor engines [6] or pulse detonation engines [7]. Since flameproof enclosures may not be able to withstand an internal explosion, holes must be big enough so that pressure does not increase beyond the enclosure limit but small enough so that the exhausted hot burnt gases cannot ignite a surrounding flammable mixture. In Internal Combustion Engines (ICEs), on the contrary, hot burnt gases jets may be used to ignite a flammable mixture: in pre-chamber ignition systems, an auxiliary charge is ignited inside a small pre-chamber linked to the main chamber of the engine by multiple ducts in order to produce hot turbulent jets. In this application, the holes need to be big enough to ensure ignition in the main chamber but small enough to produce turbulent fluctuations which speed up the main charge consumption. In all cases, the ability to predict ignition success or failure of the flamable mixture in which the hot burnt gases jets penetrate is critical for holes design.

Knowing the critical size for flame quenching in a duct [8] is not enough to establish the duct size limit that separates ignition success from ignition failure. It is not necessary that an healthy flame escapes through a hole for ignition of an outer flammable mixture to be realized: the flame can quench in the hole and still push a jet of hot gases which are able to ignite the fresh mixture depending

on the temperature, composition and dynamics of the hot jet even if it has stopped reacting [9, 10, 11, 12, 13]. Therefore, the true ignition limits are set by the aerothermochemical processes taking place in the outer atmosphere in which hot burnt gases penetrate.

Several studies have been carried out on pre-chamber/main chamber systems to investigate the effect of several parameters (ignition location, hole size, fuel type, equivalence ratio, etc.) on the ignition of a fresh mixture. Yamaguchi et al. [9] experimentally studied the effect of hole size, charge stratification and volume ratio of a divided chamber bomb filled with propane/air mixtures. They showed that the ignition pattern was greatly influenced by the hole size and the volume ratio and classified it into four categories, depending on the amount of flame kernel at the nozzle exit: chemical chain ignition, composite ignition, flame kernel ignition and flame front ignition. More recently, Sadanandan et al. [13] performed experimental investigations using hydrogen/air mixtures to gain information about the spatial and temporal evolution of the ignition process. A combination of mixing reactor model/spectroscopic simulations was used to link the observed OH LIF signals with certain states (extinction, ignition, and combustion). The influence of the hot jet temperature and speed of mixing between the burnt and fresh gases on the ignition process was highlighted: quenching of the flame inside the duct was observed by the absence of significant amount of OH radicals at the nozzle exit. Biswas et al. [12] used an experimental setup to study the effects of pressure, temperature, equivalence ratio along with geometric factors on the ignition mechanisms of hydrogen/air mixtures. They observed ignition even if the flame was quenched passing through the connecting duct. A global Damköhler number was proposed to evaluate the ignition probability. It was constructed using a chemical time scale based on the fresh premixed mixture thermochemical properties and a flow time scale based on the velocity fluctuations properties at the nozzle exit. Results showed that this number contains essential features as it successfully delineated the ignition modes and ignition limits. However, the potential heat losses to the wall of the connecting duct which lower the ignition capacity of the hot jet are a missing key parameter.

Mastorakos et al. [14] studied the pre-chamber combustion, jet injection and subsequent premixed flame initiation for ethylene and methane/air mixtures using an experimental test rig and Large Eddy Simulation (LES). They described several jet ignition phases, including the "outer flame ignition" phase that is of interest for the present work. During this phase, the main ignition sites were spotted at the tip of the transient jet. High velocities and stretch rates inhibit ignition at the sides of the jet. OH* and CH* emissions suggest quenching of the flame inside the duct, with subsequent reignition. Following this work, Allison et al. [15] used a similar setup to further investigate fundamental turbulent jet dynamics, with a particular emphasis placed on the effect of fuel type, mixture composition, orifice size, and ignition location. Qin et al. [16] investigated full ignition and flame propagation processes in a methane/air mixture using Direct Numerical Simulation (DNS) and detailed chemical kinetics. The effects of the jet on the main chamber have been categorized as chemical, thermal and potential enrichment effect due to mixture stratification. For their configuration which uses a rich mixture in the pre-chamber, the jet hot species OH, $CH_2O$, and $HO_2$ were found to play an important role in the ignition and propagation of the main chamber flame. In a similar way, limiting the DNSs to two dimensions, Benekos et al. [17] performed a parametric study to investigate the combustion phenomenology and the jet ignition process under different initial temperatures, main chamber compositions and wall boundary conditions. Several findings are relevant for the present work: the pre-chamber/main chamber interaction begins as soon as combustion develops in the pre-chamber, which generates a transient unburnt jet in the main chamber, which in turn generates strong turbulence in the region close to the outlet of the connecting duct. This first non-reactive jet has an important effect on the subsequent interaction with the hot burnt gases jet later exiting the pre-chamber. Furthermore, they showed that the hot burnt gases jet exits the pre-chamber at a temperature that can be significantly lower than the adiabatic flame temperature of the corresponding mixture due to wall heat losses. In the main chamber, the local flame structure differed strongly from that of a one-dimensional premixed laminar flame.

A large part of the ignition processes does not depend on the details of the pre-chamber design and many authors using simulations decided to study only the jet of hot burnt gases into a premixed charge. Iglesias et al. [18] used axisymmetric Navier-Stokes computations under low-Mach approximation associated with a simple one-step chemistry to investigate hot jet ignition. They proposed a critical Damköhler number whose parametric dependence is investigated. They found that the Reynolds number exerts a limited influence on this critical Damköhler number while the influence of reactant diffusivity is much more pronounced, facilitating ignition. Ghorbani et al. [19] numerically investigated jet ignition of a hydrogen/air coflow using a Probability Density Function (PDF) method to elucidate the mechanisms leading to ignition and explain the processes governing the ignition delay time and location. It was shown that mixing and chemical kinetics have a strong influence on the ignition process and that a realistic model for ignition has to account for these processes. Validi et al. [20] carried out a DNS of a statistically steady jet of hot gases interacting with a coflow of a hydrogen/air mixture. It was found that turbulence wrinkles and alters the local flame structure which differs significantly from standard turbulent premixed flames.

Sidey et al. [21] proposed an original approach, similar to the Representative Interactive Flamelet (RIF) method of Peters et al. [22, 23, 24], to study the ignition of a methane/air mixture by fully or partially burnt products: they used one-dimensional transient flamelets assuming that ignition occurs in thin layers between hot products and fresh mixture. It was shown that high scalar dissipation rates are able to freeze chemistry which is not fast enough to keep with mixing. When the degree of reaction completion in the hot products stream is decreased, ignition is harder to achieve. Application of the partially burnt hot stream flamelets to pre-chamber jet ignition cases is nevertheless disputable as the pre-chamber acts as a fully burnt gases, potentially cooled, reservoir. The present work uses an extension of this model in Section 3.1.

Despite these contributions, the effects of the jet injection speed and temperature on ignition have been rarely discussed independently: most recent

parametric studies investigated the effect of variables influencing multiple jet ignition key parameters at the same time. For example in pre-chamber/main chamber systems, decreasing the diameter of the connecting duct increases heat losses from the flowing mixture to the walls but also increases the jet injection speed because of higher overpressures in the pre-chamber. Decoupling and studying independently the effects of the jet injection speed and temperature is difficult to achieve by using experiments. Another approach is to use DNS to directly control these key parameters. Therefore, the present work uses a three-dimensional, kinetically detailed, DNS parametric study to:

- gain knowledge on the physics of ignition by a jet of hot burnt gases;
- investigate the effects of the jet injection speed and temperature on flame initiation and development;
- build and test models to predict the outcome of an ignition sequence.

The configuration is a generic case where a ducted jet of hot burnt gases enters a quiescent atmosphere filled with a premixed charge (Fig. 1). For the present study, the injected hot burnt gases have the same equivalence ratio as the atmosphere. This corresponds to a situation where the partially enclosed volume generating burnt gases is previously filled with the mixture of the atmosphere either by piston compression in ICEs or naturally in industrial safety

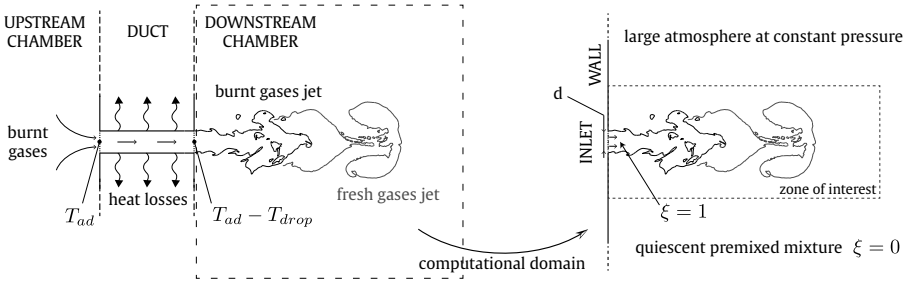


Figure 1: Left: hot burnt gases jet injection from an upstream chamber into a downstream chamber through a duct. Right: corresponding DNSs configuration. $\xi$ is the mixture fraction of gases that stem from the hot burnt gases jet.

applications.

Most existing jet ignition investigations in similar configurations [25, 26, 19, 18] have used at least one of the two simplifications that follow, which are relaxed here i) the injected jet composition corresponds to hot burnt gases at the initial time and ii) the injected gases are non-cooled: their temperature is the adiabatic flame temperature. Relaxing these simplifications is important for two reasons:

- even if injecting burnt gases right from the start of the DNSs is convenient for computation purposes, it does not correspond to reality and it affects results: combustion in an upstream partially enclosed volume first pushes out fresh gases before that burnt gases reach the inlet of the duct and are pushed out in turn, entrained by the prior flow (Fig. 2). The structure of the jet head is then different from that of a sudden starting jet because of the entrainment effects and the turbulence potentially generated by the fresh gases injection near the nozzle exit [17]. The DNSs must therefore take into account the entire injection sequence so that the jet develops as it would in real applications.

- burnt gases lose temperature to the walls when they flow through the injection hole. The temperature of the jet burnt gases $T_{inj}$ is therefore smaller than the adiabatic flame temperature $T_{ad}$. It will be shown that the difference between $T_{inj}$ and $T_{ad}$, $T_{drop} = T_{ad} - T_{inj}$ is one of the key parameters controlling the result of an ignition sequence. In piston engines using a pre-chamber for ignition, $T_{drop}$ can reach 200 K [27]. Benekos et al. [17] found even larger $T_{drop}$, up to 585 K in their simplified divided chamber setup.

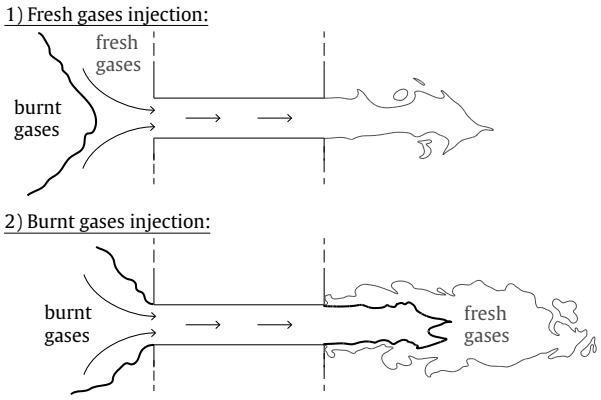


Figure 2: Typical injection sequence for ignition of fresh gases by a jet of hot burnt gases: 1) fresh gases are pushed through the duct until 2) burnt gases reach the orifice at a time $t = t_{tr}$.

## 2. Direct Numerical Simulations

### *2.1. Configuration*

#### *2.1.1. Numerical Setup*

The solver used for this work is an explicit cell-vertex massively-parallel code solving the compressible multi-species Navier-Stokes equations called AVBP [28, 29]. To solve the transport equations, a fully explicit two-step Taylor-Galerkin finite element numerical scheme is used [30] which offers third order accuracy in space and time on irregular grids. Viscosity follows a power law function of temperature. Thermal diffusivity is computed from the viscosity using a constant Prandtl number: Pr = 0.71. Species diffusion fluxes rely on Hirschfelder and Curtis approximation [31] where diffusion coefficients are computed using constant Schmidt numbers. Table 1 gives the Schmidt and Lewis numbers of the main species used for these DNSs.

#### *2.1.2. Chemistry Description*

Propane is used as fuel, air as oxidizer. Description of the chemical kinetics relies on Analytically Reduced Chemistry (ARC) whose application to reacting flows is widely described by Felden [32]. ARC mechanisms allow to accurately

describe the chemistry and contain intermediate species involved in the process of ignition by hot burnt gases [16, 15, 9, 17], keeping the computational cost at an affordable level for a three-dimensional code [33, 34, 35, 36]. The ARC mechanism is specially constructed for this work using the YARC tool [37]. Reduction starts from the San Diego mechanism [38, 39, 40]. The final ARC mechanism contains 35 species (14 of them in quasi-steady state) and 161 reactions. A full description of the ARC scheme and of its validation is included in Appendix A.

*2.1.3. Computational Domain and Resolution*

The computational domain consists of a constant pressure atmosphere in which a 4 mm diameter cylindrical jet injects the burnt gases (Fig. 1). Walls are used on all boundaries and the domain is large enough so that pressure remains almost constant during the simulations (the maximum rise in mean pressure is 0.2 Pa). The unstructured tetrahedral meshes comprise a zone of interest with a characteristic cell size of 80 $\mu$m and, thanks to the unstructured capacities of the code, much larger cell sizes are used elsewhere. To optimize the computational cost, the zone of interest is adjusted to the jet penetration length of the simulated cases. Depending on the jet injection speed and the simulation end time, different grid configurations M1 to M5 are used (Fig. 5) whose number of cells $n_{cells}$ is summarized in Table 2.

To check that the flame is correctly resolved using 80 $\mu$m cells, a one-dimensional premixed laminar flame was computed with this resolution and compared with Cantera [41] results (Appendix B.1). Furthermore, a grid independence study on the full three-dimensional DNSs was used to verify that the

| Species $k$ | $C_3H_8$ | $O_2$ | $H_2O$ | $CO_2$ | CO | $H_2$ | H | OH |
|---|---|---|---|---|---|---|---|---|
| $Sc_k$ | 1.22 | 0.74 | 0.55 | 0.94 | 0.75 | 0.20 | 0.12 | 0.49 |
| $Le_k$ | 1.72 | 1.04 | 0.77 | 1.33 | 1.05 | 0.29 | 0.17 | 0.68 |

Table 1: Schmidt $Sc_k$ and Lewis $Le_k$ numbers used for some of the species used for the DNS of propane/air flames.

80 $\mu$m grid was sufficient to capture the aerothermochemical processes during ignition (Appendix B.2).

*2.1.4. Initial Conditions*

The atmosphere is initially at rest, filled with a perfectly premixed propane/air lean mixture at an equivalence ratio $\Phi_u = 0.8$, a temperature $T_u = 298$ K and a pressure $P_a = 1$ atm. The lean equivalence ratio corresponds to one of our target applications: ICEs equipped with pre-chamber. Atmospheric conditions were selected to make the three-dimensional DNS parametric study computationally feasible. Although this does not cover the entire operating range of ICEs, main ignition mechanisms are not expected to differ from those at ICE relevant conditions.

*2.1.5. Boundary Conditions*

The walls of the computational domain are maintained at the initial temperature $T_u$. A Navier-Stokes characteristic boundary condition [42, 8, 43] is used to handle the inlet injection and limit acoustic reflections. No arbitrary turbulence is injected into the jet so that potential turbulent structures develop naturally in the atmosphere. To mimic the ignition sequence produced by the jet issuing from a pre-chamber (Fig. 2), the DNS boundary condition at the jet inlet uses two phases in time:

1) first, fresh gases are injected from the start of injection time $t_{si}$ to the transition time $t_{tr}$;
2) then, burnt gases are injected until the end of injection time $t_{ei}$.

The injection timing is chosen so as to correspond to a typical injection due to combustion in a small partially enclosed volume [27]. Appendix C shows that

| | M1a | M1b | M2a | M2b | M2c | M3 | M4 | M5 |
|---|---|---|---|---|---|---|---|---|
| $n_{cells} \cdot 10^{-6}$ | 217 | 272 | 358 | 435 | 786 | 449 | 696 | 769 |

Table 2: Number of cells in the different grid configurations.

$t_{tr}$ plays a limited role on the ignition results. Appendix D shows that the injection of burnt gases is long enough so that the jet reaches a quasi-steady state where the ignition outcome no longer depends on the duration of the burnt gases injection. Velocity and temperature profiles at the jet injection section are quasi flat profiles to correspond to a short injection tube from a pre-chamber where boundary layers do not have time to develop. The injected burnt gases are equilibrium combustion products from a cold mixture initially at $\Phi_u$, $T_u$ and $P_a$ which is burnt and then cooled by a fixed temperature drop $T_{drop}$ before entering the DNS domain. The chemical composition of the injected burnt and potentially cooled gases is also changed to correspond to equilibrium values at temperature $T_{inj} = T_{ad} - T_{drop}$.

Mathematically, this results in several functions to describe the spatial and temporal evolution of the primitive variables at the inlet:

- the radial profile of the inlet axial velocity reads

$$U(r,t) = f_U(t)\hat{U}(r), \tag{1}$$

where $r$ is the duct radial distance from its axis, $t$ is the simulation time, $\hat{U}(r)$ is the spatial velocity profile

$$\hat{U}(r) = U_{inj}\left[1 - \left(\frac{r}{d/2}\right)^N\right], \tag{2}$$

where $U_{inj}$ is the target injection speed, $d$ is the duct diameter, $N$ is the dampening function coefficient, and $f_U$ is the temporal velocity function

$$f_U(t) = \frac{1}{2}\left[\tanh\left(\frac{t - t_{si}}{K_U}\right) - \tanh\left(\frac{t - t_{ei}}{K_U}\right)\right], \tag{3}$$

where $K_U$ is a parameter which controls the transition width;

- the temperature profile reads

$$T(r,t) = f_b(t)T_b(r) + (1 - f_b(t))T_u, \tag{4}$$

where $T_b(r)$ is the spatial burnt gases temperature profile

$$T_b(r) = T_u + (T_{inj} - T_u)\left[1 - \left(\frac{r}{d/2}\right)^N\right], \tag{5}$$

where $T_{inj}$ is the target hot burnt gases temperature

$$T_{inj} = T_{ad} - T_{drop}, \tag{6}$$

and $f_b(t)$ is the temporal burnt gases function

$$f_b(t) = \frac{1}{2}\left[\tanh\left(\frac{t - t_{tr}}{K_{tr}}\right) + 1\right], \tag{7}$$

where $K_{tr}$ is a parameter which controls the transition width;

- the species mass fraction profile reads

$$Y_k(r,t) = f_b(t)Y_{k,eq}(r) + (1 - f_b(t))Y_{k,u}, \tag{8}$$

where the k subscript refers to the $k^{th}$ species, u subscript refers to the fresh gases and $Y_{k,eq}(r)$ are the species mass fraction at equilibrium at the temperature $T_b(r)$.

Figure 3 and 4 show the spatial and temporal profiles resulting from the parameters chosen for this work (Tab. 3). $K_U$ is chosen such that the temporal velocity transition width defined as

$$ep^t_{f_U} = \frac{\max(f_U) - \min(f_U)}{\left|\max\left(\frac{df_U}{dt}\right)\right|}, \tag{9}$$

is equal to 40 $\mu$s which allows relatively smooth transition from zero velocity to jet injection. $K_{tr}$ is adjusted to produce a spatial burnt gases transition width defined as

$$ep^x_{f_b} = \frac{\max(f_b) - \min(f_b)}{\left|\max\left(\frac{df_b}{dx}\right)\right|}, \tag{10}$$

equal to the laminar flame thermal thickness $\delta^0_L$.

| $t_{si}$ [ms] | $t_{tr}$ [ms] | $t_{ei}$ [ms] | $K_U$ [-] | $K_{tr}$ [-] | $N$ [-] |
|---|---|---|---|---|---|
| 0.05 | 0.35 | 1.05 | $2 \cdot 10^{-5}$ | $\delta^0_L/(2U_{inj})$ | 20 |

Table 3: Parameters used to describe the inlet injection.

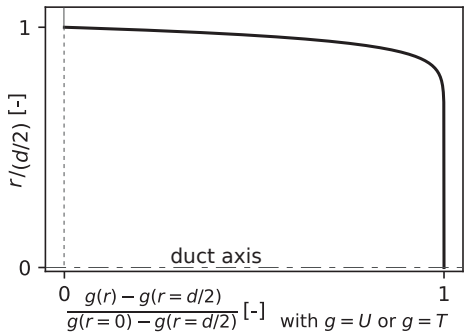


Figure 3: Spatial inlet profile for axial velocity and temperature.

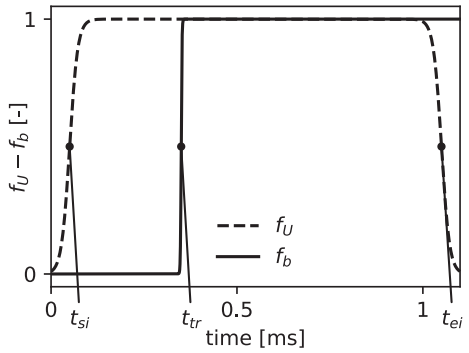


Figure 4: Temporal inlet functions for injection speed ($f_U$) and burnt gases ($f_b$, steers both temperature and mass fractions).

#### 2.1.6. Variability

When the flow becomes turbulent, several realizations of an ignition sequence may differ. However, the conditions encountered along the jet interface exhibit all possible states for every simulation even when the realizations differ slightly. The main outcome (ignition or no ignition) then does not change: ignition may not occur at the same point but if it must occur for this regime, it will. This was checked by repeating the same simulation including various perturbations in spatial discretization (e.g. Appendix B) or in injection timing (e.g. Appendix C and Appendix D): the overall result was unaffected.

### 2.2. Results

#### 2.2.1. Ignition Domain

Ignition sequences have been simulated for multiple combinations of inlet injection speed $U_{inj}$ and temperature drop $T_{drop}$. Corresponding jet Reynolds numbers $Re_x$ defined as

$$Re_x = \frac{U_{inj} d}{\nu_x}, \tag{11}$$

where $\nu$ is the kinematic viscosity of the injected gases and the $x$ subscript refers to the nature of the injected gases (burnt, $b$ or unburnt, $u$), are displayed in Fig. 5 along with ignition results. Ignition sequences are classified as successful if the initiated flame kernels are sufficiently strong to induce self-sustained flames after that burnt gases injection stops and as failed otherwise. Ignition is governed by the competition between the rate of heat production due to chemical reactions of the fresh mixture diffusing into the hot jet and the rate of heat losses due to thermal diffusion. When the jet velocity increases, the diffusion process responsible for the transport of reactants toward the hot burnt gases becomes stronger. However, thermal diffusion also increases. It actually increases faster than molecular diffusion does, for fuels having a Lewis number greater than unity as for propane (Table 1). Hence, chemistry may not be able to compensate for heat losses any more (black crosses in Fig. 5). More intuitively, a too large temperature drop $T_{drop}$ for the injected hot burnt gases weakens chemistry and leads to ignition failure. The $T_{drop}$ maximum value for ignition success decreases

with increasing speed until ignition is no longer possible (here, $U_{inj}$ above 200 m/s).

DNS allows to analyse the local flame structure during the ignition sequence: Fig. 6 displays the maximum Heat Release Rate (HRR) reached in the whole domain versus time for multiple cases. This local maximum HRR overshoots the maximum HRR found in a one-dimensional premixed laminar flame $\max(\mathrm{HRR})^{1\mathrm{DL}}$, showing that some additional mixing may take place before combustion actually starts and/or that the flow alters the internal flame structure from its canonical laminar form.

Local HRR close to or higher than $\max(\mathrm{HRR})^{1\mathrm{DL}}$ do not necessary imply that global ignition will eventually be reached (see cases [$U_{inj} = 200$ m/s, $T_{drop} = 100$ K], [$U_{inj} = 250$ m/s, $T_{drop} = 0$ K] and [$U_{inj} = 300$ m/s, $T_{drop} = 0$ K]). Even if small local ignition spots are formed, the reactive flow structure may be disorganized by high turbulence intensity and not be able to give rise to self-supported propagating flames because of too many heat losses to the surrounding: these zones may be below the critical radius for flame kernel propagation.

### *2.2.2. Analysis of Ignition Sequences*

*Low Injection Speed.* For low injection speeds, no high-intensity turbulence structure is found (Fig. 7) and the flame elements are "flamelet-like". The burnt gases jet develops in a mushroom shape and detaches from the hole lips when injection stops. For $T_{drop} = 0$, 100, 200 and 300 K, the rolled-up toroidal structure at the jet head is a favourable place for flame kernel development, driven by large scale engulfment of fresh gases into the toroidal vortex core resulting in large scale mixing of fresh gases and hot burnt gases. At this low speed, it is necessary to increase the injected burnt gas cooling to $T_{drop} = 400$ K to obtain a failed ignition sequence. The failure is not due to local flame kernels which ignite but are too small to grow: it is due to the fact that chemical reactions are not excited by the cooled jet and ignition does not occur anywhere in the flow.

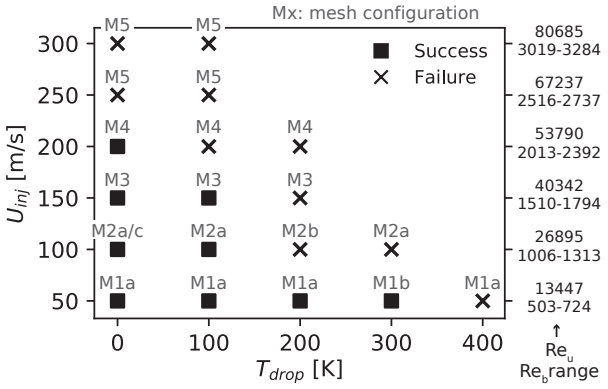


Figure 5: DNS results: ignition map of the studied cases in a $U_{inj} - T_{drop}$ diagram. The mesh configuration used for each case is specified above the markers. Jet Reynolds numbers are given on the right.

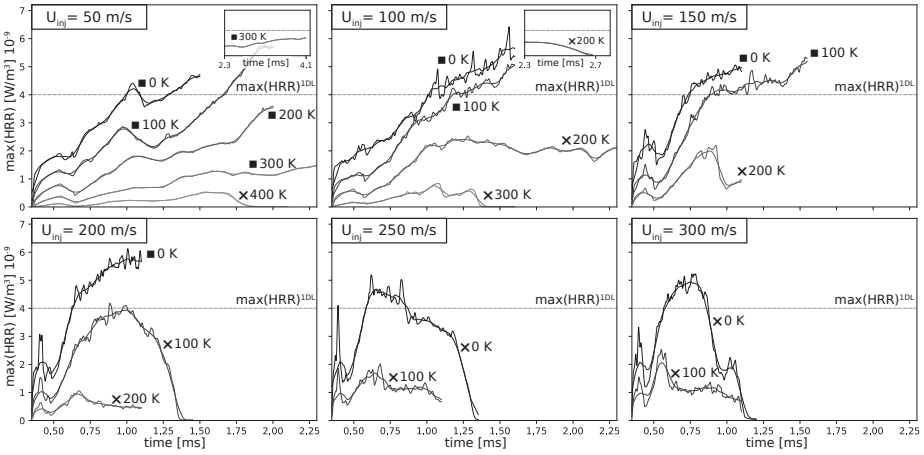


Figure 6: Instantaneous and moving average maximum HRR in the domain for various values of inlet injection speed $U_{inj}$ and temperature drop $T_{drop}$.

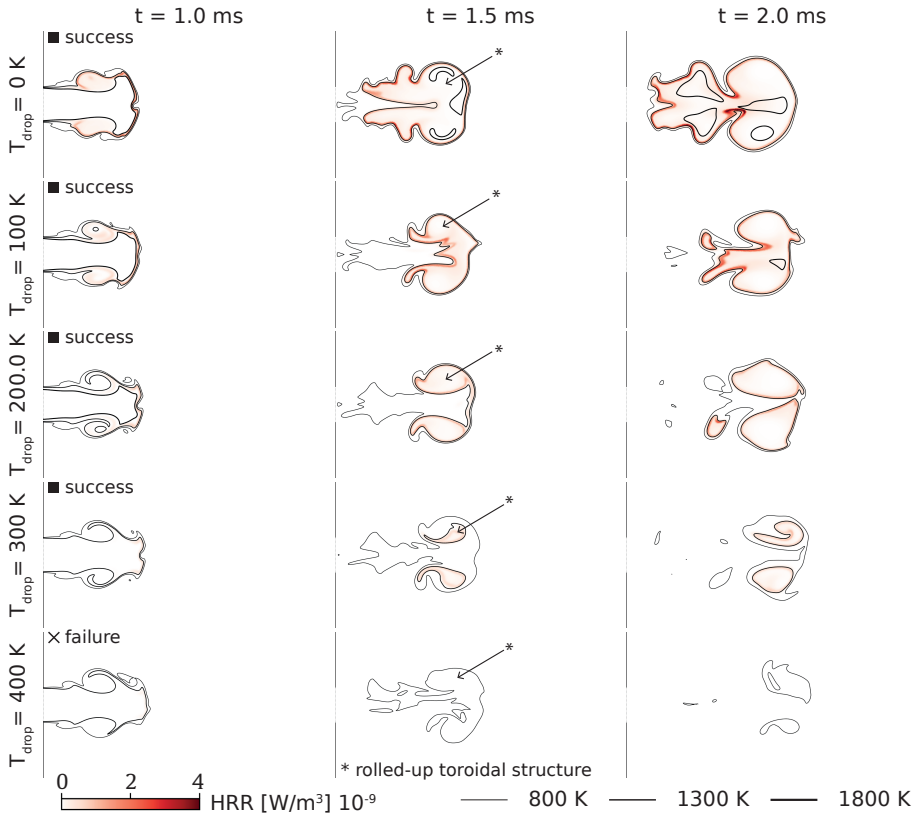


Figure 7: Planar cut in the jet axis coloured by the HRR with three isolines of temperature. $U_{inj} = 50$ m/s.

*Moderate Injection Speed.* For higher injection speeds, turbulent structures show up and strongly disrupt the jet structure and the flame development (Fig. 8) where no flamelet structure seems to appear. Moderate injection speed encompasses here $U_{inj} = 100$ to 200 m/s. Only $U_{inj} = 150$ m/s results are shown but cases $U_{inj} = 100$ and 200 m/s qualitatively show similar results. The initial jet head has similarities with the low injection speed cases. Quickly, the higher generated turbulence creates a disordered jet with intense mixing by small scale structures and the large scale vortex at the jet head is broken up. Ignition occurs within the inner volume of the intense mixing zone at the jet head in a broadened/distributed reaction mode already observed in ICEs [27]. For $T_{drop} = 200$ K, chemistry is not fast enough to compensate for heat losses due to intense mixing and ignition fails. A parallel can be drawn with the findings of Shy et al. [44, 45, 46] that revealed turbulent-distributed flame kernels during the ignition process of a premixed charge by a spark discharge under intense turbulence regime. In this distributed ignition mode, significantly higher ignition energies must be provided to ensure the development of turbulent flame kernels because of increased heat losses due to kernels disruption and turbulence.

*High Injection Speed.* For $U_{inj} > 200$ m/s, ignition never happens due to high levels of heat losses exerted by the intense turbulence (Fig. 9). Only small reactive kernels appear and they are quickly extinguished by the flow so that global ignition of the atmosphere is never reached.

### *2.2.3. Chemical Explosive Mode Analysis*

Chemical Explosive Mode Analysis (CEMA) is a useful diagnostic tool developed by Lu et al. [47] to identify flame and ignition structure in DNS of complex flows [48, 49, 50, 51, 52, 53, 54]. It is based on the eigenanalysis of the Jacobian of the local chemical source terms in the governing equations of a reacting flow

$$\frac{D\boldsymbol{\omega}(\boldsymbol{y})}{Dt} = \boldsymbol{J}_{\boldsymbol{\omega}} \frac{D\boldsymbol{y}}{Dt} = \boldsymbol{J}_{\boldsymbol{\omega}}(\boldsymbol{\omega} + \boldsymbol{s}), \tag{12}$$

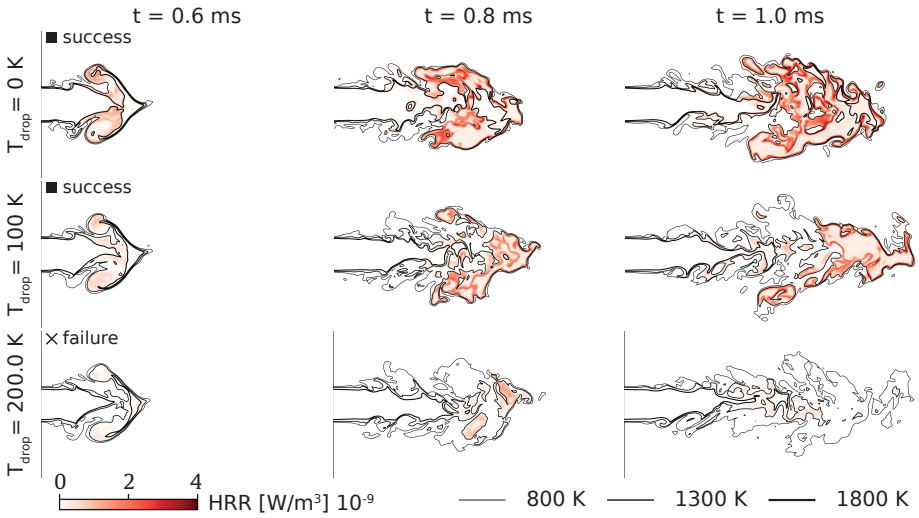


Figure 8: Planar cut in the jet axis coloured by the HRR with three isolines of temperature. $U_{inj} = 150$ m/s.

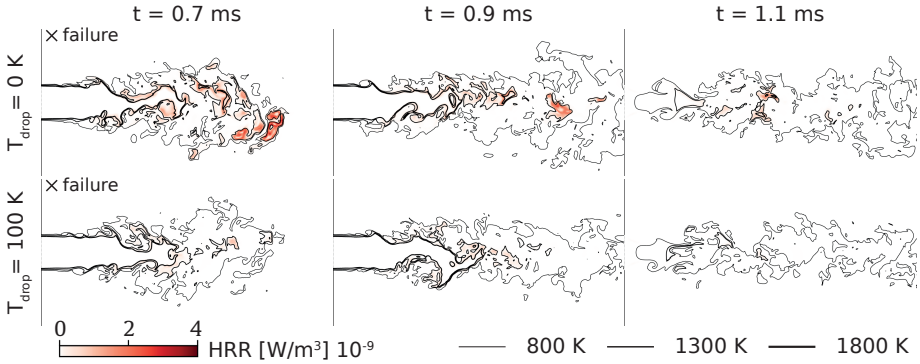


Figure 9: Planar cut in the jet axis coloured by the HRR with three isolines of temperature. $U_{inj} = 250$ m/s.

where $\boldsymbol{y}$ is the vector of the local thermochemical dependent variables including temperature and species mass fractions, $\boldsymbol{\omega}$ is the chemical source term, $\boldsymbol{s}$ is the diffusion source term and $\boldsymbol{J}_\omega$ is the Jacobian matrix of the chemical source terms

$$\boldsymbol{J}_\omega = \frac{\partial \boldsymbol{\omega}}{\partial \boldsymbol{y}}. \tag{13}$$

A Chemical Explosive Mode (CEM) exists if $\boldsymbol{J}_\omega$ has an unstable eigenvalue characterized by a positive real part $\lambda_e$, related to the chemical Jacobian $\boldsymbol{J}_\omega$ by

$$\lambda_e = \boldsymbol{b}_e \cdot \boldsymbol{J}_\omega \cdot \boldsymbol{a}_e, \tag{14}$$

where $\boldsymbol{a}_e$ and $\boldsymbol{b}_e$ are right and left eigenvectors associated with $\lambda_e$, respectively. A CEM indicates the propensity of a local mixture to ignite in an lossless environment where $\boldsymbol{s} \ll \boldsymbol{\omega}$. If multiple CEMs are present, $\lambda_e$ refers to the largest eigenvalue by recognizing that ignition is controlled by the fastest CEM. Validation and more details on the practical implementation are included in Appendix E.

*Local combustion mode.* Xu et al. [50] introduced a local combustion mode indicator $\alpha$ by projecting Eq. 12 in the direction of the fastest CEM

$$\frac{D\phi_\omega}{Dt} = \lambda_e \phi_\omega + \lambda_e \phi_s + \frac{D\boldsymbol{b}_e}{Dt} \cdot \boldsymbol{\omega}(\boldsymbol{y}), \tag{15}$$

where the projected chemical ($\phi_\omega$) and diffusion ($\phi_s$) source terms are defined as

$$\phi_\omega \equiv \boldsymbol{b}_e \cdot \boldsymbol{\omega}, \tag{16}$$

$$\phi_s \equiv \boldsymbol{b}_e \cdot \boldsymbol{s}, \tag{17}$$

and defining the local combustion mode indicator

$$\alpha = \phi_s / \phi_\omega. \tag{18}$$

This ratio compares the relative alignment of diffusion and chemical source terms contributions with the fastest CEM and can be interpreted as follows:

- if $\alpha > 1$, diffusion dominates chemistry in the direction of the fastest CEM and promotes the ignition of the mixture;

- if $\alpha < -1$, diffusion dominates chemistry in the opposite direction of the fastest CEM and inhibits the ignition of the mixture;

- if $|\alpha| \leq 1$ chemistry dominates diffusion in the direction of the fastest CEM and promotes the ignition of the mixture.

In premixed flames, the local combustion mode indicator $\alpha$ discriminates between the preheat zone where $\alpha > 1$ and the reaction zone where $|\alpha| \leq 1$ (Fig. 10). Fig. 11 shows the local combustion mode indicator $\alpha$ for explosive mixture (i.e. $\lambda_e > 0$) for low, moderate and high injection speed cases without any $T_{drop}$. For low injection speed, the reaction zone is thin and not much distorted by the flow. The internal structure of the flames is very similar to a one-dimensional premixed laminar flame as shown by the one-dimensional plot through the interface between the fresh gases and the burnt gases. On the other hand, $\alpha$ demonstrates the broadening of the reaction zone for higher injection speeds already depicted in Fig 8. $|\alpha| \leq 1$ zones become thickened and/or distributed. For $U_{inj} = 50$ m/s, projected diffusion source terms mostly act in favour of the fastest CEM as in the preheat zone of a premixed laminar flame where heat and combustion products diffuse back into the unburnt mixture leading to self-supported flames. For higher speeds, $\alpha < -1$ zones appear where diffusion acts against the fastest CEM. In these zones, ignition is inhibited by the flow. For $U_{inj} = 250$ m/s (ignition failure), $|\alpha| \leq 1$ zones are quickly broken up and $\alpha < -1$ zones dominate. More generally, as expected for ignition by hot burnt gases, diffusion plays an important role in the ignition process as shown by large $|\alpha| > 1$ zones.

## 3. Models

While the previous DNSs reveal much of the physics controlling hot jet ignition, they are too complicated to be used in practice for any design process. However, they can be used to build much simpler models as shown now. Modelling the scenario of Fig. 1 requires assumptions on the mechanisms controlling

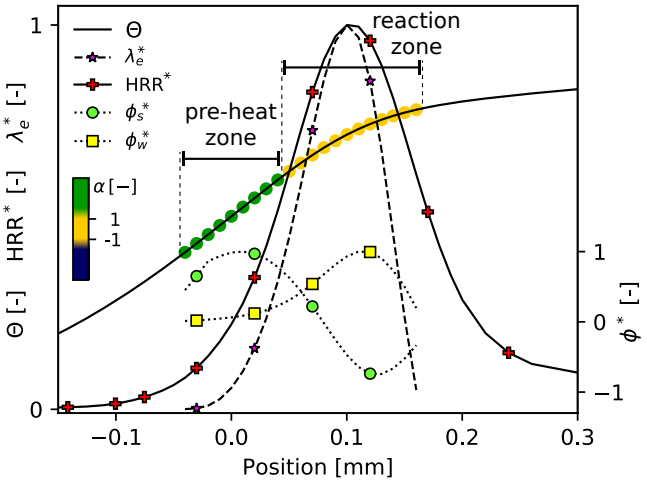


Figure 10: Example of CEMA applied to a one-dimensional premixed laminar flame at 1 atm, unburnt temperature $T_u$ and equivalence ratio $\Phi_u$. Stared variables are normalized by their maximum absolute value, $\Theta$ is the reduced temperature profile such that $\Theta(T = T_u) = 0$ and $\Theta(T = T_{ad}) = 1$.

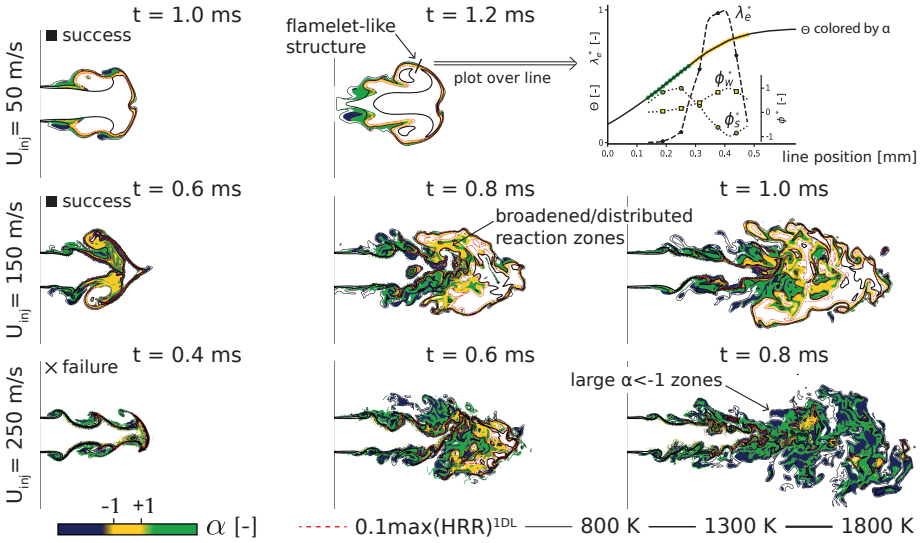


Figure 11: Planar cut along the jet axis coloured by the local combustion mode indicator $\alpha$ with three isolines of temperature and one isoline of HRR. Upper right plot reveals a CEMA flame structure similar to a one-dimensional premixed laminar flame using a line cut through the three-dimensional flame. Stared variables are normalized by their maximum absolute value, $\Theta$ is the reduced temperature. $T_{drop} = 0$ K.

ignition. These mechanisms may change when jet properties vary: for low injection speeds, chemistry evolves in a shorter time scale than mixing making flamelet approaches probably adequate; on the other hand, for larger injection speeds, mixing and chemical time scales may become comparable which suggests that models not relying on any flame structure assumption may be more appropriate. Therefore, two models are tested here: the first one (called Unsteady Flamelet for Ignition Prediction (UFIP), Section 3.1) is a variation of the classical RIF proposed by N. Peters [22, 23, 24] and assumes that the ignition process takes place (or not) in a thin, flamelet-like front. The second one (called Convected Open Reactor (COR), Section 3.2) adopts a Lagrangian vision to relax the flamelet assumption: it views the ignition process as the evolution of an open well-stirred reactor convected into the chamber, where fresh gases and hot products mix at a certain rate and ignite or not. In each of these models, the jet is assumed to act as an infinite source of ignition sites having the same aerothermochemical properties. As a consequence, a single ignition site can be used as a representation of the multiple ignition attempts. This implies that these models can only be used to model jets that have reached a quasi-steady state (as is the case in the DNSs of this work) where ignition no longer depends on the duration of the injection.

### *3.1. Unsteady Flamelet for Ignition Prediction (UFIP) Model*

As established by Peters [22], if chemistry is fast compared to transport processes, combustion takes place within asymptotically thin layers embedded in the flow. Applying this concept to jet ignition, the boundary of the jet may be seen as a continuous interface strained and convected by the flow [21] (Fig. 12). Along this interface, the motion of any fluid line segment may be decomposed into translation, rotation and strain (given by the relative change in length of the line segment). In the reference frame of the fluid line segment, the only effect of motion that will be apparent is that of strain [55]. Translation and rotation may change the mixture that the flame front encounters, but only strain will alter the internal flame structure. These line segments embedded

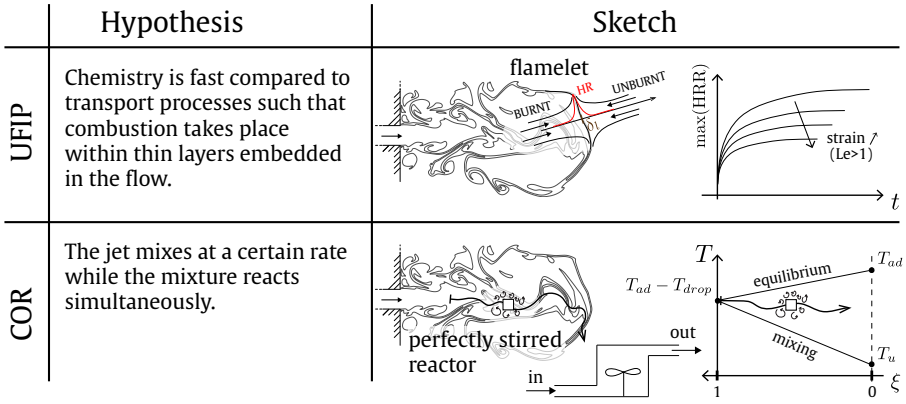


Figure 12: The two models developed from DNS to describe ignition by a hot burnt gases jet.

between the cold unburnt and the hot burnt gases are called flamelets, their inner structure is one-dimensional and time-dependent. They lose heat only to the unburnt gases side and can receive heat and chemically active radicals from the burnt gases side. The concept of the UFIP model follows this idea: one representative unsteady strained flamelet is supposed to capture what is happening at the boundary of the jet in terms of ignition. In this work, the open-source software Ember [56] is used to compute this unsteady flamelet with high efficiency [57], assuming an infinite reservoir of burnt gases on the product side of the counterflow flame.

A flame in this configuration can never be completely extinguished because there will always be a region of contact between reactants and products: a threshold of HRR is needed to distinguish between flamelets able to globally ignite the fresh mixture or not. This threshold is arbitrarily set to half of the max(HRR) found in a one-dimensional premixed laminar flame at the same fresh gases conditions. As the temperature drop increases at the burnt gases side of the flamelets, chemistry is weakened and the time to reach this threshold increases (Fig. 13). For a fuel with Lewis number greater than unity, heat diffuses more quickly than mass, reducing the temperature in the reaction zone when strain increases and therefore the HRR decreases monotonically with the strain rate $a$ [58].

Hot burnt gases jet ignition exhibits different structural characteristics with increasing turbulence intensity starting from wrinkled flames to a more disorganized combustion pattern where small eddies broke/broaden the reaction zone (Section 2). Results from UFIP can only be compared to DNSs lying in the flamelet regime where the reaction zones are not distributed/broadened and the burnt gases are not highly fragmented in space. This limit the range of application of the UFIP model to the $U_{inj} = 50$ m/s cases only.

The UFIP model requires a relation between the stretch to impose to the representative flamelet—which reduces to the strain in its zero-curvature planar configuration—and the aerodynamic features of the jet. In a three-dimensional flow field, at each point of an isosurface of progress variable $c$, the flame stretch is defined as

$$\kappa = -\boldsymbol{nn} : \nabla \boldsymbol{u} + \boldsymbol{\nabla} \cdot \boldsymbol{u} + S_d(\boldsymbol{\nabla} \cdot \boldsymbol{n}), \tag{19}$$

where $\boldsymbol{n}$ is the flame normal pointing toward the fresh gases

$$\boldsymbol{n} = -\frac{\boldsymbol{\nabla} c}{|\boldsymbol{\nabla} c|}, \tag{20}$$

$\boldsymbol{u}$ is the flow velocity and $S_d$ is the flame displacement speed

$$S_d = \frac{1}{|\boldsymbol{\nabla} c|} \frac{Dc}{Dt}. \tag{21}$$

The DNSs data can be post processed to evaluate the level of stretch that the interface between burnt and fresh gases undergoes. However, there are several obstacles: first, the flamelets at the interface of the jet are subject to a wide range of local stretches (Fig. 14). Second, the strain rate of the interface changes in time as it is randomly disturbed by the flow. Constructing a single strain rate to apply to a flamelet supposed to represent what is happening at the whole interface of the jet becomes difficult: locally, a thin layer may undergo low strain rates and lead to ignition even if globally, the average strain rate is high. Moreover, a flame may survive at higher unsteady strain rates than it would at steady strain rates [59]. These difficulties prevent from using the unsteady and heterogeneous flow field of the DNSs to establish a relation between the UFIP strain to be applied and the jet characteristics. Here, to bypass this problem, a

simpler approach is used: an equivalent strain rate $a^e$ is defined as the steady strain applied to UFIP flamelets which would be equivalent to what happens to the unsteady thin layers featuring large strain variation. $a^e$ is supposed to scale as the inverse of a jet flow time scale defined as the ratio between the duct diameter and the injection speed such that

$$a^e = K^{\mathrm{UFIP}} \frac{U_{inj}}{d}, \tag{22}$$

where $K^{\mathrm{UFIP}}$ is a scaling constant. The UFIP model is in good agreement with the DNSs for $K^{\mathrm{UFIP}} = 0.06$ which results in $a^e = 750$ s$^{-1}$ for $U_{inj} = 50$ m/s, close to all of the most probable stretch values encountered in the DNSs for this injection speed (Fig. 14). For this strain rate, UFIP predicts an ignition failure for $T_{drop} > 300$ K using the arbitrary threshold $0.5\mathrm{max}(\mathrm{HRR})^{\mathrm{1DL}}$ to distinguish between ignition success and failure (Fig. 13).

### *3.2. Convected Open Reactor (COR) Model*

The UFIP model is limited to flamelet-like thin reaction fronts, which restricts its range of application to low injection speeds. As an alternative, a more general modelling approach (the COR model) is explored now (Fig. 12). It consists in following an open reactor—small enough to be homogeneous—, convected into the chamber: hot burnt gases mix at a certain rate with the cold fresh gases within the open reactor and chemistry inside the reactor can be tracked using a simple Ordinary Differential Equation (ODE) solver with complex chemistry. In this approach, the mixture fraction between the hot jet and the cold gases $\xi$ in the open reactor changes according to a mixing rate: it starts at $\xi = 1$ in the injected burnt gases jet and goes to $\xi = 0$ as the reactor is convected inside the chamber and mixes with the fresh gases. The details of the convection movement are unimportant once the evolution of $\xi$ is specified.

The balance equations are those describing the evolution of an open system at constant pressure. The mass balance equation reads

$$\frac{dm}{dt} = \dot{m}^{in} - \dot{m}^{out}, \tag{23}$$

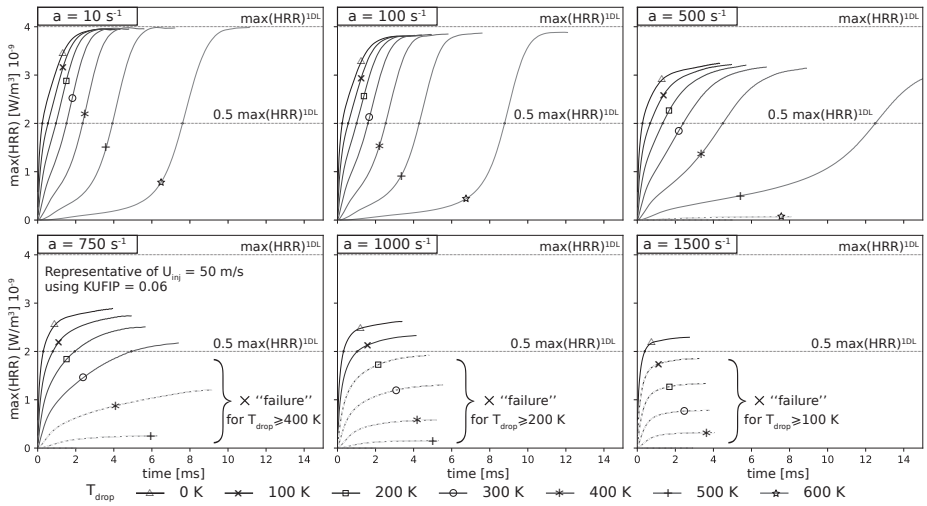


Figure 13: Temporal evolution of the maximum HRR in one-dimensional strained unsteady flamelets for multiple strain rates $a$ and temperature drops $T_{drop}$. Dashed lines do not cross the $0.5\max(\mathrm{HRR})^{1\mathrm{DL}}$ horizontal line. It is assumed that the corresponding flamelets are too weak to lead to global ignition in jet ignition cases.

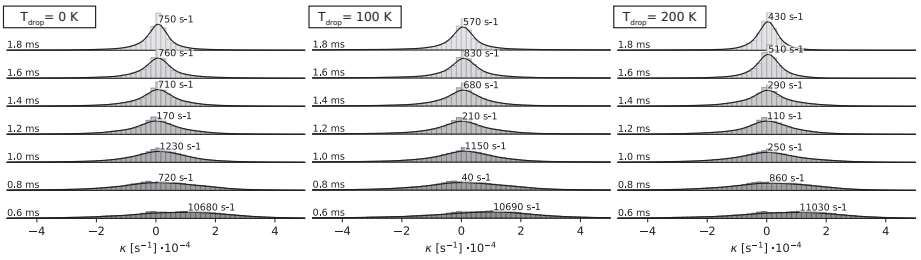


Figure 14: Kernel density approximation and histogram of the stretch computed using $0.1 < c < 0.9$ isosurfaces. Annotated stretch are most probable values. $U_{inj} = 50$ m/s.

where $m$ is the reactor mass, $\dot{m}^{in}$ is the mass flow entering the reactor (i.e. that comes from the flammable atmosphere) while $\dot{m}^{out}$ is the mass flow leaving the reactor. The rate of entrainment of the cold mixture into the system $\theta$ is defined as

$$\theta = \frac{\dot{m}_{in}}{m}. \tag{24}$$

The species balance equations for the convected reactor read

$$\frac{dY_k}{dt} = \theta \left(Y_k^{in} - Y_k\right) + \frac{rT}{P}\dot{\omega}_k, \tag{25}$$

where $Y_k$ is the mass fraction of the k$^{\text{th}}$ species, $T$ is the temperature, $r$ is the specific gas constant, $P$ is the pressure and $\dot{\omega}_k$ is the chemical source term of the k$^{\text{th}}$ species. The energy balance equation can be rearranged to describe the evolution of temperature

$$\frac{dT}{dt} = \frac{1}{Cp}\left[\theta \sum_k Y_k^{in}\left(h_k^{in} - h_k\right) - \frac{rT}{P}\sum_k h_k \dot{\omega}_k\right], \tag{26}$$

where $Cp$ and $h$ are the specific heat capacity at constant pressure and the enthalpy per unit mass, respectively. The evolution of the mixture fraction $\xi$ is described by a passive scalar balance equation similar to Eq. 25 without chemical source term

$$\frac{d\xi}{dt} = \theta\left(\xi^{in} - \xi\right) = -\xi\theta, \tag{27}$$

since $\xi^{in} = 0$ (the fresh gases entering the reactor have a zero mixture fraction). Thus, using chain's rule, the system evolution can be described as a function of $\xi$ by a set of two equations:

$$\frac{dY_k}{d\xi} = \frac{dY_k}{dt}\frac{dt}{d\xi} = -\frac{1}{\xi}\left(Y_k^{in} - Y_k\right) - \frac{rT}{\theta\xi P}\dot{\omega}_k \tag{28}$$

and

$$\frac{dT}{d\xi} = \frac{dT}{dt}\frac{dt}{d\xi} = -\frac{1}{\xi Cp}\sum_k Y_k^{in}\left(h_k^{in} - h_k\right) + \frac{rT}{\xi\theta CpP}\sum_k h_k\dot{\omega}_k. \tag{29}$$

This model was used to aid the interpretation of experimental results for burnt gases jet ignition [13], namely the OH LIF signals. A similar concept was also used to examine the evolution of a hot air kernel ejected into a stratified coflow

[60]. Here, the aim is to predict ignition. Balance equations 28 and 29 are integrated thanks to a SciPy [61] wrapped ODE solver. Thermodynamic and kinetic parameters needed in each equation are computed using Cantera [41].

The weak part of the COR model is that all mixing aspects are hidden in the mixing rate $\theta$ (Eq. 24) which becomes the most critical parameter of the model. The mixing rate $\theta$ should be equal to zero in the fresh and in the burnt gases (i.e. $\theta(\xi = 1) = \theta(\xi = 0) = 0$) and should be non-zero in the mixing zones. Since mixing occurs by removal of scalar variance and the scalar dissipation rate of $\xi$ $\chi_\xi$ represents the rate at which the fluctuation of $\xi$ are destroyed, it is assumed here that the mixing rate $\theta$ is linked to the rate at which mixing occurs in the jet and therefore to $\chi_\xi$ so that a linear relation between the mixing rate $\theta$ and the scalar dissipation rate of $\xi$ is used to close the model. To finalize the model for $\theta$, the distribution of $\chi_\xi$ as a function of $\xi$ in the DNSs (Fig. 15) can be used. $\chi_\xi = f(\xi)$ seems to follow a parabolic curve such that $\theta$ may be modelled using the function

$$\theta = \theta_0 4\xi(1-\xi), \tag{30}$$

where $\theta_0$ is the maximum mixing rate supposed to scale as the inverse of a jet flow time scale such that

$$\theta_0 = K^{\mathrm{COR}} \frac{U_{inj}}{d}, \tag{31}$$

where $K^{\mathrm{COR}}$ is a scaling constant. Figure 16 shows an example of COR model results for $T_{drop} = 100$ K using various values for the maximum mixing rate

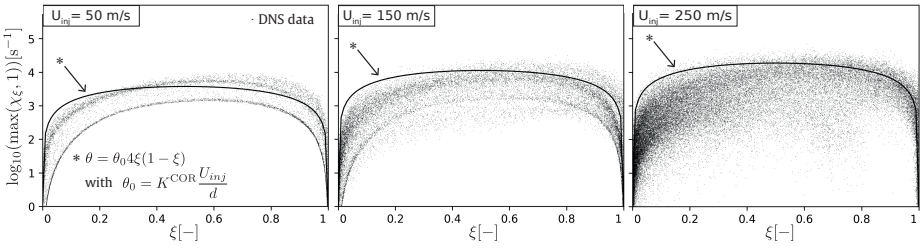


Figure 15: Scatter plot of the scalar dissipation rate of the jet mixture fraction $\chi_\xi$ versus the corresponding value of jet mixture fraction $\xi$ for the DNSs alongside the $\theta$ modelling function (Eq. 30) with $K^{\mathrm{COR}} = 0.3$ (—). $T_{drop} = 0$ K, $t = 0.4$ ms.

$\theta_0$. As expected, for large $\theta_0$, chemistry is not fast enough to balance the cooling effect of the entrainment of fresh gases. Temperature quickly falls to the fresh gases temperature: it is an ignition failure. For smaller $\theta_0$, the rate of combustion heating exceeds the rate of entrainment cooling and temperature rises to the burnt gases temperature: it is an ignition success. The COR model captures the essence of the phenomena at play here: ignition is controlled by the balance between the rate of combustion heating due to the combustion of the entrained fresh fuel and the rate of mixing cooling due to the entrainment of fresh gases. From this, it is possible to compute $\theta_0^{crit}$, the critical mixing rate which separates ignition success from ignition failure. Using $K^{\mathrm{COR}} = 0.3$ in Eq. 31 the ignition limit established by the COR model is in fairly good agreement with all DNS results (Fig. 17). This suggests that, despite its simplicity, the COR model (which accounts for complex chemistry effects) captures ignition limits reasonably. Figure 18 shows guidelines for a practical use of the COR model.

## 4. Conclusion

Multiple DNSs of hot burnt gases jet ignition sequence have been performed, varying the jet injection speed and temperature. Increasing the heat energy supply by increasing the jet injection speed does not necessary favour ignition: higher turbulence generation due to higher jet injection speed may prevent ignition to be reached. This is a very important information for ICEs designers, seeking to increase turbulence to speed up the main charge consumption through flame wrinkling. This work has highlighted a jet injection speed limit beyond which ignition would no longer be possible. This jet injection speed limit decreases when the temperature drop that the burnt gases undergo through the duct increases. This highlights the importance of taking into account heat losses in the small gaps from which jets issue, too often overlooked in jet ignition studies.

For modelling perspectives, this work has brought some fundamental knowledge on hot burnt gases jet ignition. The flame structure was found to be

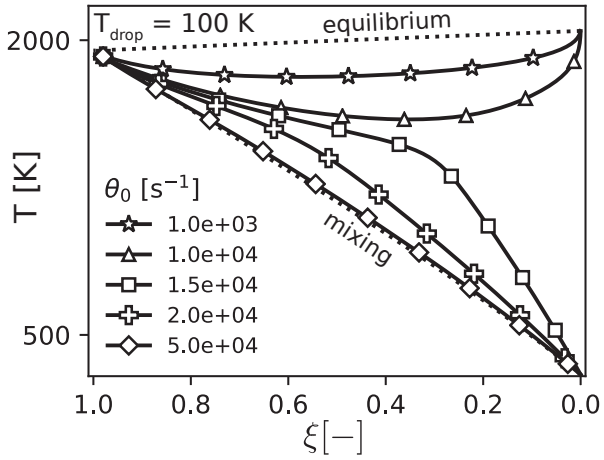


Figure 16: Evolution of the temperature inside multiple COR model open reactors for different maximum mixing rates $\theta_0$. The trajectories start at $\xi = 1$ (in the hot burnt gases jet) and go to $\xi = 0$ as the system fills with fresh gases. The mixing line corresponds to an infinitely fast mixing case while the equilibrium line corresponds to an infinitely fast chemistry case.

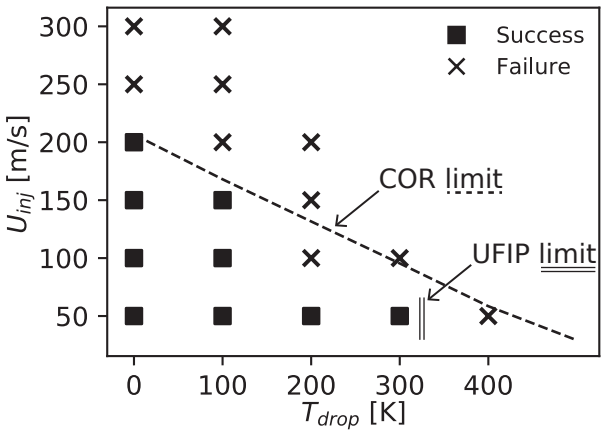


Figure 17: Ignition map of the studied cases (DNS results) together with the UFIP model ignition limit for $K^{\mathrm{UFIP}} = 0.06$ and the COR model ignition limit for $K^{\mathrm{COR}} = 0.3$.

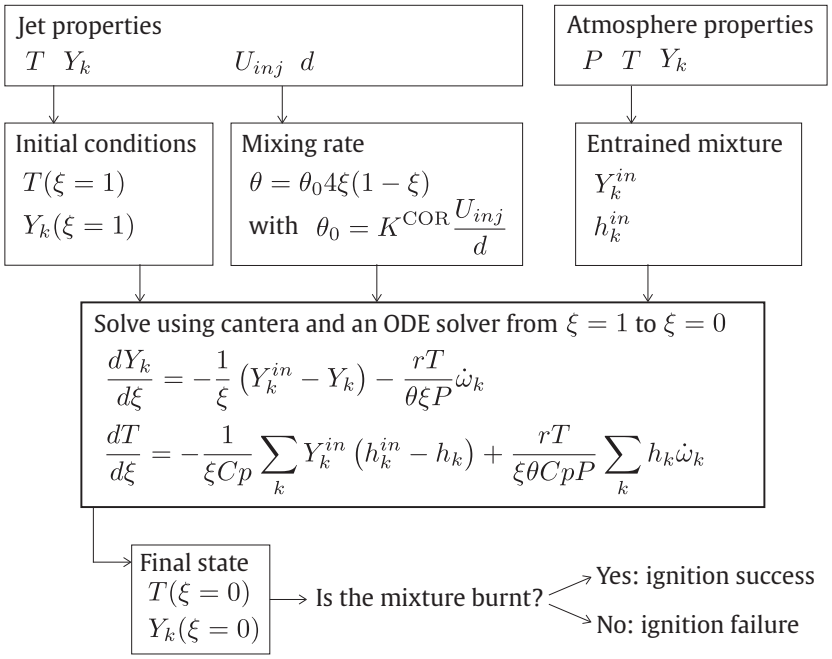


Figure 18: Flowchart showing the practical use of the COR model.

strongly impacted by the jet injection speed. Under low-intensity and large-scale turbulence conditions, turbulence wrinkles the flames but is not able to penetrate their preheat and reaction zones. In this condition, segments of the wrinkled flames can be considered as laminar flamelets. For high-intensity and small-scale turbulence, the entire structure of the reaction zone is substantially distorted by the penetration of small eddies. Thus, the reaction zone is broadened and/or distributed. This results in a combustion mode fundamentally distinct from that of laminar flamelets. This broadened/distributed reaction zone regime—already revealed in ICE turbulent jet ignition [27]—is depicted through visual analysis of the HRR field and supported by the CEMA diagnostic tool.

Two models have been evaluated using the DNSs as reference: the UFIP model where ignition takes place within thin layers embedded in the flow and the COR model where the system mixes at a certain rate while the mixture reacts simultaneously. These models are simple one-dimensional and zero-dimensional

models but they both integrate a key element which is a precise description of chemistry through complex chemical kinetics. Major drawbacks of the UFIP model are i) the need of a representative steady strain rate and ii) the flamelet regime assumption. The COR model adopts an opposite modeling strategy by assuming perfect mixing and no flamelet structure as the UFIP model does. The ignition limits given by the COR model are in good agreement with the DNSs showing that it is a good candidate to predict the ignition of a flammable atmosphere by jets of hot burnt gases for which flamelet approaches (such as UFIP) are not adequate as many regimes encountered during these ignition sequences, especially at large injection speeds, do not fall in the flamelet regime. Future work will integrate this model in ICE turbulent jet ignition modelling to track misfires and optimize the design of this technology.

**Acknowledgements**

This work was granted access to the high performance computing resources of TGCC ("Très Grand Centre de calcul du Commissariat à l'énergie atomique et aux énergies alternatives") under the allocation number 2019204881 attributed by PRACE (Partnership for Advanced Computing in Europe) and the allocation number A0072B10157 attributed by GENCI ("Grand Équipement National de Calcul Intensif"). Quentin Malé is the recipient of the CIFRE ("Conventions Industrielles de Formation par la Recherche") Ph.D. research fellowship number 2017/0295 attributed by ANRT ("Association Nationale de la Recherche et de la Technologie").

**Declaration of Interests**

The authors declare that they have no known competing financial interests or personal relationships that could have appeared to influence the work reported in this paper.

## References


[1] H. Phillips, A Summary of Research into the Basic Principles of Flameproof Enclosure, Proc. Inst. Mech. Eng 184 (9) (1969) 23–30.

[2] C. Grantham, Electrical safety in hazardous environments, Int. J. Electr. Power Energy Syst. 7 (4) (1985) 194–200.

[3] J. Benajes, R. Novella, J. Gomez-Soriano, P. J. Martinez-Hernandiz, C. Libert, M. Dabiri, Evaluation of the passive pre-chamber ignition concept for future high compression ratio turbocharged spark-ignition engines, Appl. Energy 248 (2019) 576–588.

[4] C. E. C. Alvarez, G. E. Couto, V. R. Roso, A. B. Thiriet, R. M. Valle, A review of prechamber ignition systems as lean combustion technology for SI engines, Appl. Therm. Eng. 128 (2018) 107–120.

[5] E. Toulson, H. J. Schock, W. P. Attard, A Review of Pre-Chamber Initiated Jet Ignition Combustion Systems, SAE Powertrains Fuels & Lubricants Meeting (2010), paper 2010-01-2263.

[6] S. Wijeyakulasuriya, I. Perera, M. Nalim, Mixing and Ignition Potential of Transient Confined Turbulent Jet in a Wave Rotor Combustor, 46th AIAA/ASME/SAE/ASEE Joint Propulsion Conference & Exhibit (2012), paper 2010-7042.

[7] D. Lieberman, K. Parkin, J. Shepherd, Detonation Initiation by a Hot Turbulent Jet for use in Pulse Detonation Engines, 38th AIAA/ASME/SAE/ASEE Joint Propulsion Conference & Exhibit (2002), paper 2002-3909.

[8] T. Poinsot, D. Veynante, Theoretical and Numerical Combustion, R. T. Edwards, Philadelphia, PA, USA, 2001.

[9] S. Yamaguchi, N. Ohiwa, T. Hasegawa, Ignition and burning process in a divided chamber bomb, Combust. Flame 59 (1985) 177–187.

[10] H. Phillips, On the transmission of an explosion through a gap smaller than the quenching distance, Combust. Flame 7 (1963) 129–135.

[11] H. G. Wolfhard, A. E. Bruszak, The passage of explosions through narrow cylindrical channels, Combust. Flame 4 (1960) 149–159.

[12] S. Biswas, S. Tanvir, H. Wang, L. Qiao, On ignition mechanisms of premixed CH4/air and H2/air using a hot turbulent jet generated by prechamber combustion, Appl. Therm. Eng. 106 (2016) 925–937.

[13] R. Sadanandan, D. Markus, R. Schießl, U. Maas, J. Olofsson, H. Seyfried, M. Richter, M. Aldén, Detailed investigation of ignition by hot gas jets, Proc. Combust. Inst. 31 (1) (2007) 719–726.

[14] E. Mastorakos, P. Allison, A. Giusti, P. De Oliveira, S. Benekos, Y. Wright, C. Frouzakis, K. Boulouchos, Fundamental Aspects of Jet Ignition for Natural Gas Engines, 13th International Conference on Engines & Vehicles (2017), paper 2017-24-0097.

[15] P. M. Allison, M. de Oliveira, A. Giusti, E. Mastorakos, Pre-chamber ignition mechanism: Experiments and simulations on turbulent jet flame structure, Fuel 230 (2018) 274–281.

[16] Q. Fei, A. Shah, H. Zhi-wei, P. Li-na, P. Tunestal, B. Xue-Song, Detailed numerical simulation of transient mixing and combustion of premixed methane/air mixtures in a pre-chamber/main-chamber system relevant to internal combustion engines, Combust. Flame 188 (2018) 357–366.

[17] S. Benekos, C. E. Frouzakis, G. K. Giannakopoulos, M. Bolla, Y. M. Wright, K. Boulouchos, Prechamber ignition: An exploratory 2-D DNS study of the effects of initial temperature and main chamber composition, Combust. Flame 215 (2020) 10–27.

[18] I. Iglesias, M. Vera, A. L. Sánchez, A. Liñán, Numerical analyses of deflagration initiation by a hot jet, Combust. Theory Model. 16 (6) (2012) 994–1010.

[19] A. Ghorbani, G. Steinhilber, D. Markus, U. Maas, Ignition by transient hot turbulent jets: An investigation of ignition mechanisms by means of a PDF/REDIM method, Proc. Combust. Inst. 35 (2) (2014) 2191–2198.

[20] A. Validi, F. Jaberi, Numerical Study of Turbulent Jet Ignition in a Lean Premixed Configuration, Flow Turbul. Combust. 100 (1) (2017) 197–224.

[21] J. A. M. Sidey, E. Mastorakos, Pre-Chamber Ignition Mechanism: Simulations of Transient Autoignition in a Mixing Layer Between Reactants and Partially-Burnt Products, Flow Turbul. Combust. 101 (4) (2018) 1093–1102.

[22] N. Peters, Laminar flamelet concepts in turbulent combustion, Symp. (Int.) Combust. 21 (1) (1988) 1231–1250.

[23] C. Felsch, M. Gauding, C. Hasse, S. Vogel, N. Peters, An extended flamelet model for multiple injections in DI Diesel engines, Proc. Combust. Inst. 32 (2) (2009) 2775–2783.

[24] C. Hergart, H. Barths, N. Peters, Modeling the Combustion in a Small-Bore Diesel Engine Using a Method Based on Representative Interactive Flamelets, International Fuels & Lubricants Meeting & Exposition (1999), paper 1999-01-3550.

[25] M. E. Feyz, V. R. Hasti, J. P. Gore, A. Chowdhury, M. R. Nalim, Scalar predictors of premixed gas ignition by a suddenly-starting hot jet, Int. J. of Hydrog. Energy (2019) 1–14.

[26] S. Fischer, D. Markus, U. Maas, Numerical investigation of the ignition of diethyl ether/air and propane/air mixtures by hot jets, J. Loss Prev. Process Ind. 49 (2017) 1–25.

[27] Q. Malé, G. Staffelbach, O. Vermorel, A. Misdariis, F. Ravet, T. Poinsot, Large Eddy Simulation of Pre-Chamber Ignition in an Internal Combustion Engine, Flow Turbul. Combust. 131 (1) (2019) 1–19.

[28] T. Schonfeld, M. Rudgyard, Steady and Unsteady Flow Simulations Using the Hybrid Flow Solver AVBP, AIAA J. 37 (11) (1999) 1378–1385.

[29] L. Y. M. Gicquel, N. Gourdain, J.-F. Boussuge, H. Deniau, G. Staffelbach, P. Wolf, T. Poinsot, High performance parallel computing of flows in complex geometries, Comptes Rendus Mécanique 339 (2-3) (2011) 104–124.

[30] O. Colin, M. Rudgyard, Development of High-Order Taylor-Galerkin Schemes for LES, J. Comput. Phys. 162 (2) (2000) 338–371.

[31] J. O. Hirschfelder, C. F. Curtiss, R. B. Bird, Molecular Theory of Gases and Liquids, Wiley, New York, USA, 1954.

[32] A. Felden, Development of Analytically Reduced Chemistries and Applications in Large Eddy Simulations of Turbulent Combustion, Ph.D. thesis, Université de Toulouse, 2017.

[33] T. Jaravel, E. Riber, B. Cuenot, G. Bulat, Large Eddy Simulation of an industrial gas turbine combustor using reduced chemistry with accurate pollutant prediction, Proc. Combust. Inst. 36 (3) (2016) 1–9.

[34] B. Rochette, F. Collin-Bastiani, L. Gicquel, O. Vermorel, D. Veynante, T. Poinsot, Influence of chemical schemes, numerical method and dynamic turbulent combustion modeling on LES of premixed turbulent flames, Combust. Flame 191 (2018) 417–430.

[35] A. Felden, E. Riber, B. Cuenot, Impact of direct integration of Analytically Reduced Chemistry in LES of a sooting swirled non-premixed combustor, Combust. Flame 191 (2018) 270–286.

[36] A. Felden, L. Esclapez, E. Riber, B. Cuenot, H. Wang, Including real fuel chemistry in LES of turbulent spray combustion, Combust. Flame 193 (2018) 397–416.

[37] P. Pepiot-Desjardins, Automatic Strategies to Model Transportation Fuel Surrogates, Ph.D. thesis, Stanford University, 2008.

[38] J. C. Prince, F. A. Williams, Short chemical-kinetic mechanisms for low-temperature ignition of propane and ethane, Combust. Flame 159 (7) (2012) 2336–2344.

[39] P. Saxena, F. A. Williams, Testing a small detailed chemical-kinetic mechanism for the combustion of hydrogen and carbon monoxide, Combust. Flame 145 (1-2) (2006) 316–323.

[40] M. V. Petrova, F. A. Williams, A small detailed chemical-kinetic mechanism for hydrocarbon combustion, Combust. Flame 144 (3) (2006) 526–544.

[41] D. G. Goodwin, R. L. Speth, H. K. Moffat, B. W. Weber, Cantera: An Object-oriented Software Toolkit for Chemical Kinetics, Thermodynamics, and Transport Processes, V2.4.0, 10.5281/zenodo.251665.

[42] T. J. Poinsot, S. K. Lelef, Boundary conditions for direct simulations of compressible viscous flows, J. Comput. Phys. 101 (1) (1992) 104–129.

[43] N. Guezennec, T. Poinsot, Acoustically Nonreflecting and Reflecting Boundary Conditions for Vortcity Injection in Compressible Solvers, AIAA J. 47 (7) (2009) 1709–1722.

[44] C. C. Huang, S. S. Shy, C. C. Liu, Y. Y. Yan, A transition on minimum ignition energy for lean turbulent methane combustion in flamelet and distributed regimes, Proc. Combust. Inst. 31 (1) (2007) 1401–1409.

[45] S. S. Shy, W. T. Shih, C. C. Liu, More on Minimum Ignition Energy Transition for Lean Premixed Turbulent Methane Combustion in Flamelet and Distributed Regimes, Combust. Sci. Technol. 180 (10-11) (2008) 1735–1747.

[46] S. S. Shy, C. C. Liu, W. T. Shih, Ignition transition in turbulent premixed combustion, Combust. Flame 157 (2) (2010) 341–350.

[47] T. F. Lu, C. S. Yoo, J. H. Chen, C. K. Law, Three-dimensional direct numerical simulation of a turbulent lifted hydrogen jet flame in heated

coflow: a chemical explosive mode analysis, J. Fluid Mech. 652 (2010) 45–64.

[48] C. S. Yoo, T. Lu, J. H. Chen, C. K. Law, Direct numerical simulations of ignition of a lean n-heptane/air mixture with temperature inhomogeneities at constant volume: Parametric study, Combust. Flame 158 (9) (2011) 1727–1741.

[49] Z. Luo, C. S. Yoo, E. S. Richardson, J. H. Chen, C. K. Law, T. Lu, Chemical explosive mode analysis for a turbulent lifted ethylene jet flame in highly-heated coflow, Combust. Flame 159 (1) (2012) 265–274.

[50] X. Chao, P. Ji-Woong, Y. C. Sang, C. J. H, L. Tianfeng, Identification of premixed flame propagation modes using chemical explosive mode analysis, Proc. Combust. Inst. 37 (2) (2018) 2407–2415.

[51] K. Aditya, A. Gruber, C. Xu, T. Lu, A. Krisman, M. R. Bothien, J. H. Chen, Direct numerical simulation of flame stabilization assisted by auto-ignition in a reheat gas turbine combustor, Proc. Combust. Inst. 37 (2) (2019) 2635–2642.

[52] O. Schulz, E. Piccoli, A. Felden, G. Staffelbach, N. Noiray, Autoignition-cascade in the windward mixing layer of a premixed jet in hot vitiated crossflow, Combust. Flame 201 (2019) 215–233.

[53] O. Schulz, N. Noiray, Combustion regimes in sequential combustors: Flame propagation and autoignition at elevated temperature and pressure, Combust. Flame 205 (2019) 253–268.

[54] R. Shan, C. S. Yoo, J. H. Chen, T. Lu, Computational diagnostics for n-heptane flames with chemical explosive mode analysis, Combust. Flame 159 (10) (2012) 3119–3127.

[55] Y. Marzouk, Unsteady Strained Flames: Fundamentals and Numerical Modeling, Lecture in Fundamentals and Modeling in Combustion, Massachusetts Institute of Technology, 2001.

[56] R. L. Speth, Ember: a quasi-one-dimensional, unsteady flame solver, V1.4.0, 10.5281/zenodo.1004753.

[57] A. E. Long, R. L. Speth, W. H. Green, Ember: An open-source, transient solver for 1D reacting flow using large kinetic models, applied to strained extinction, Combust. Flame 195 (2018) 1–12.

[58] C. Petrov, A. Ghoniem, An unsteady strained flame model for turbulent combustion simulations, 32nd Aerospace Sciences Meeting and Exhibit (1994).

[59] H. N. Najm, R. W. Schefer, R. B. Milne, C. J. Mueller, K. D. Devine, S. N. Kempka, Numerical and Experimental Investigation of Vortical Flow-Flame Interaction, Report No. SAND98-8232, Sandia National Laboratories, Livermore, CA, USA, 1998.

[60] B. Sforzo, J. Kim, J. Jagoda, J. Seitzman, Ignition Probability in a Stratified Turbulent Flow With a Sunken Fire Igniter, J. Eng. Gas Turbine Power 137 (1) (2014)

[61] E. Jones, T. Oliphant, P. Peterson, others, SciPy: Open source scientific tools for Python, www.scipy.org, 2001.

[62] P. Pepiot-Desjardins, H. Pitsch, An efficient error-propagation-based reduction method for large chemical kinetic mechanisms, Combust. Flame 154 (1-2) (2008) 67–81.

[63] T. Løvås, D. Nilsson, F. Mauss, Automatic reduction procedure for chemical mechanisms applied to premixed methane/air flames, Proc. Combust. Inst. 28 (2) (2000) 1809–1815.

[64] K. E. Niemeyer, N. J. Curtis, pyJac, V1.0.6, 10.5281/zenodo.1004753.

[65] K. E. Niemeyer, N. J. Curtis, C.-J. Sung, pyJac: Analytical Jacobian generator for chemical kinetics, Comput. Phys. Commun. 215 (2017) 188–203.

[66] E. Anderson, Z. Bai, C. Bischof, S. Blackford, J. Demmel, J. Dongarra, J. Du Croz, A. Greenbaum, S. Hammarling, A. McKenney, D. Sorensen, LAPACK Users' Guide, Society for Industrial and Applied Mathematics, Philadelphia, PA, USA, 1999.

## Appendix A. Analytical Reduced Chemistry Mechanism for Propane Air Flames

A set of canonical zero- or one-dimensional configurations is used to steer the reduction process towards an accurate ARC mechanism. Here, the configurations include one-dimensional premixed laminar flames and zero-dimensional auto-igniting homogeneous reactors at the thermodynamic conditions of this work. Starting from the detailed San Diego mechanism [38, 39, 40], a skeletal reduction is performed first: unimportant species and reactions are removed from the detailed mechanism using the Directed Relation Graph with Error Propagation (DRGEP) method [62]. The resulting skeletal mechanism is comprised of 35 species and 161 reactions. Then, 14 species are identified as being Quasi Steady State (QSS) species by the Level Of Importance (LOI) criterion [63]. The resulting ARC mechanism retains 21 transported species and 14 QSS species.

For the conditions of this work (pressure $P_a = 1$ atm, unburnt temperature $T_u = 298$ K and equivalence ratio $\Phi_u = 0.8$), the relative error on the laminar flame speed is equal to 3.4 %. The temporal evolution of the consumption speed of unsteady strained flamelets is predicted with less than 10 % relative error (Fig. A.19). The relative errors on the auto-ignition times stay below 10 % (Fig. A.20). To further evaluate the accuracy of the ARC mechanism applied to ignition by hot burnt gases, the behaviour of homogeneous mixtures of fresh and burnt gases are studied. Ignition times (Fig. A.21) and the times to go from 10 to 90 % temperature increment (Fig. A.22) are fairly well reproduced.

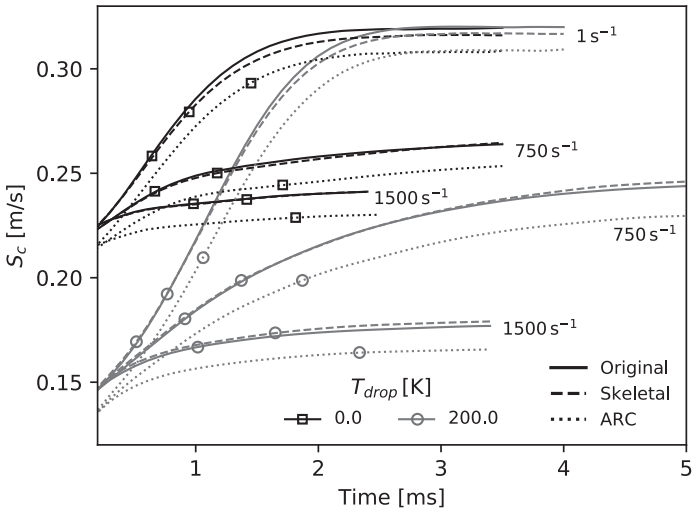


Figure A.19: Temporal evolution of the consumption speed $S_c$ for strained flames at 1 atm, unburnt temperature $T_u$ and equivalence ratio $\Phi_u$. Original, skeletal and ARC mechanisms.

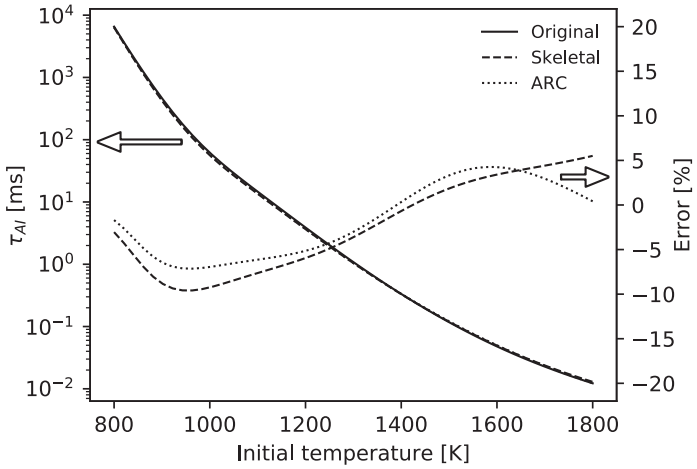


Figure A.20: Auto-ignition times $\tau_{AI}$ of homogeneous unburnt mixtures at 1 atm and equivalence ratio $\Phi_u$. Original, skeletal and ARC mechanisms. Associated errors relative to the original mechanism.

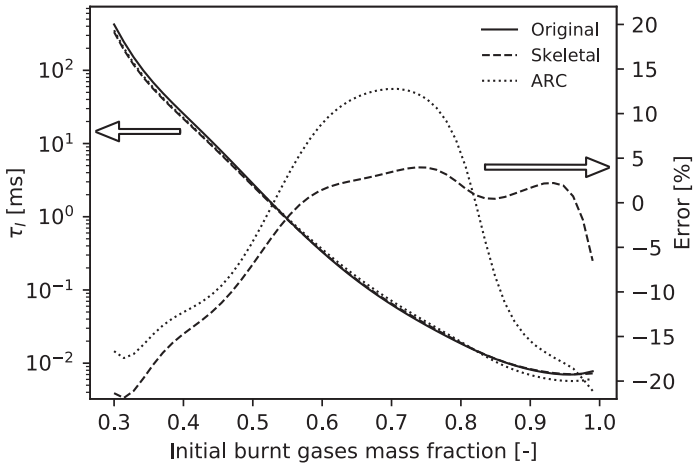


Figure A.21: Ignition times $\tau_I$ of mixtures of unburnt and burnt gases at 1 atm, unburnt temperature $T_u$ and equivalence ratio $\Phi_u$. Burnt gases are product of fresh gases equilibrium. Original, skeletal and ARC mechanisms. Associated errors relative to the original mechanism.

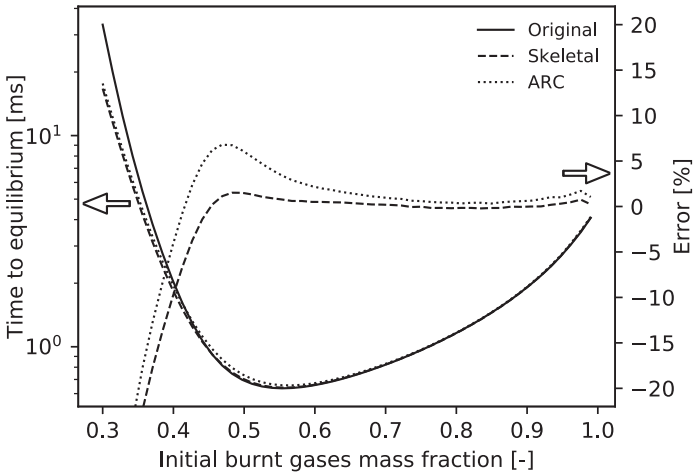


Figure A.22: Times to go from 10 to 90 % temperature increment for mixtures of unburnt and burnt gases at 1 atm, unburnt temperature $T_u$ and equivalence ratio $\Phi_u$. Burnt gases are product of fresh gases equilibrium. Original, skeletal and ARC mechanisms. Associated errors relative to the original mechanism.

## Appendix B. Grid Resolution

### *Appendix B.1. One-dimensional Flame*

For the conditions of this work (pressure $P_a = 1$ atm, unburnt temperature $T_u = 298$ K and equivalence ratio $\Phi_u = 0.8$), the thermal flame thickness of the propane/air premixed laminar flame is 420 $\mu$m. To check that the flame is correctly resolved using 80 $\mu$m cell sizes, a one-dimensional premixed laminar flame was computed with this resolution and compared with Cantera [41] results (Fig. B.23). Temperature, species and HRR profiles are consistent with the Cantera flame.

### *Appendix B.2. Three-dimensional reactive flow*

A grid refinement step from a cell size of 80 $\mu$m to 50 $\mu$m was carried out to check grid independency for the case $U_{inj} = 100$ m/s, $T_{drop} = 0$ K. It was achieved by refining the zone of interest only, leading to 786 million cells (grid M2c in Table 2).

The maximum HRR in the domain, tracker of the evolution of local reactive regions, is almost unaffected by the grid refinement (Fig. B.24). More globally, the averaged HRR in the domain shows a similar trend during ignition and is then slightly impacted by the cell size. This demonstrates that the ignition period is relatively unaffected by the grid refinement starting with a cell size of 80 $\mu$m.

## Appendix C. Influence of the Fresh Gases Injection Duration

A change in the injection transition time $t_{tr}$ from 0.35 ms to 0.65 ms was carried out to ensure that it has little impact on the results (Fig. 2). This change is done on the case $U_{inj} = 100$ m/s, $T_{drop} = 0$ K. The maximum HRR in the domain remains unaffected by the fresh gases injection duration (Fig. C.25). The averaged HRR in the domain shows similar trend during ignition and then slightly deviates due to the chaotic nature of the turbulent flow.

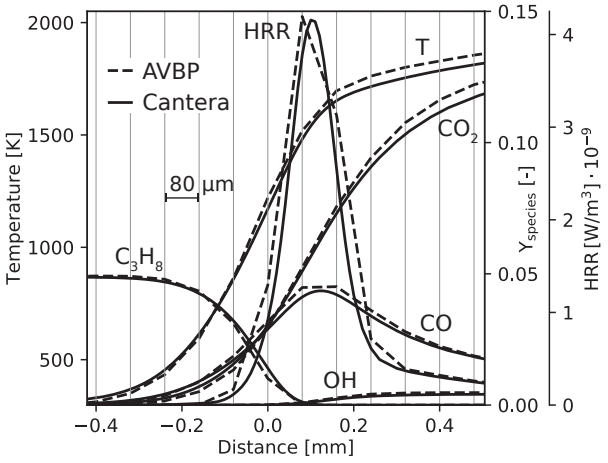


Figure B.23: One-dimensional premixed laminar flame computed using AVBP and Cantera at 1 atm, unburnt temperature $T_u$ and equivalence ratio $\Phi_u$. Vertical thin lines indicate the AVBP grid points. Axial distance is relative to the inflexion point of the temperature profile.

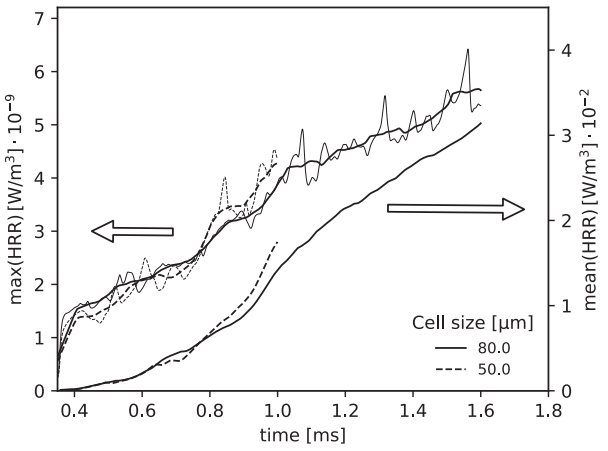


Figure B.24: Instantaneous and moving average maximum HRR alongside volume mean HRR in the domain for $U_{inj} = 100$ m/s, $T_{drop} = 0$ K and two different grid cell sizes.

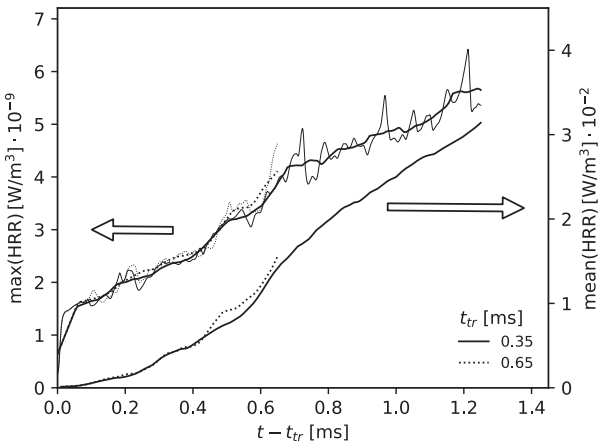


Figure C.25: Instantaneous and moving average maximum HRR alongside volume mean HRR in the domain for $U_{inj} = 100$ m/s, $T_{drop} = 0$ K and two different transition times $t_{tr}$ from fresh gases to hot burnt gases injection.

## Appendix D. Assessment of the Quasi-Steady State of the Burnt Gases Jet

Several end of injection times $t_{ei}$ have been used (0.85, 1.05 and 1.25 ms) to ensure that the burnt gases jet has reached a quasi-steady state using $t_{ei} = 1.05$ ms in the parametric study. Figure D.26 shows the chemical activity in the domain for the case $U_{inj} = 100$ m/s, $T_{drop} = 0$ K. The fact that the mean HRR increases with $t_{ei}$ shows that a longer burnt gases injection brings more ignition sites and therefore more reactive flame surface in the domain. However, the main outcome of the jet ignition sequence is not affected by the change in burnt gas injection duration. The maximum HRRs follow a similar trend and the atmosphere is ignited regardless of the end of injection time. Same conclusion is drawn for failed ignition case (Fig. D.27) where ignition failure occurs regardless of the end of injection time: a very large number of ignition attempts has taken place so that if the ignition has not succeeded, it will never succeed. The jet is therefore assumed to have reached a quasi-steady state for $t_{ei} = 1.05$ ms.

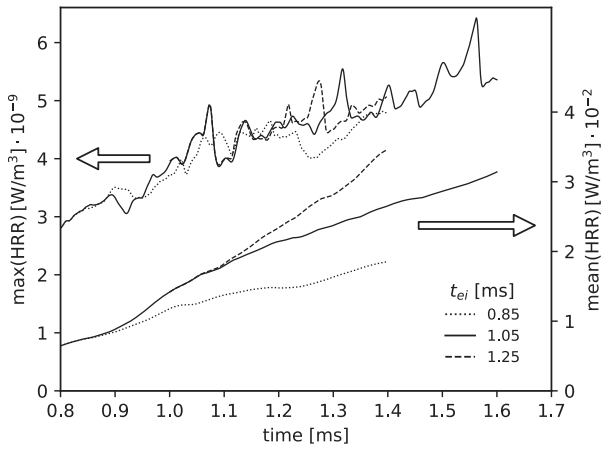


Figure D.26: Instantaneous maximum HRR alongside volume mean HRR in the domain for $U_{inj} = 100$ m/s, $T_{drop} = 0$ K and three different end of injection times $t_{ei}$.

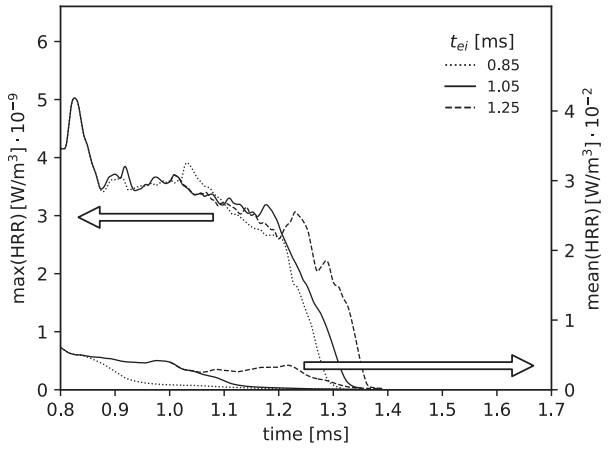


Figure D.27: Instantaneous maximum HRR alongside volume mean HRR in the domain for $U_{inj} = 250$ m/s, $T_{drop} = 0$ K and three different end of injection times $t_{ei}$.

## Appendix E. Chemical Explosive Mode Analysis Numerical Implementation

CEMA requires the computation of the Jacobian of the local chemical source terms $\boldsymbol{J}_\omega$ (Eq. 13). While the open-source software pyJac [64] offers optimized analytical generation of Jacobian matrices for classical chemical mechanisms [65], it is not directly applicable to ARC mechanisms where only transported species are included in the governing equations of the reacting flow (Eq. 12). To bypass this obstacle, first order finite differences are used in this work to approximate the Jacobian matrix of the local ARC mechanism chemical source terms. Eigenvalues and eigenvectors are computed using LAPACK [66].

To validate the method, CEMA is applied to a one-dimensional premixed laminar flame using both pyJac and finite differences for the skeletal mechanism and only finite differences for the ARC mechanism (Fig. E.28). The different approaches give very similar results, allowing finite differences to be used in this work. The freely propagating premixed flame is characterized by the lack of CEM in the unburnt mixture. $\lambda_e$ shows up in the preheat zone of the flame driven by back diffusion of energy and radicals as shown by the projected diffusion source terms $\phi_s$ which dominates the projected chemical source terms $\phi_\omega$. $\lambda_e$ continues to grow in the reaction zone where $\phi_\omega \gg \phi_s$ before disappearing, separating pre- and post-ignition zones [47].

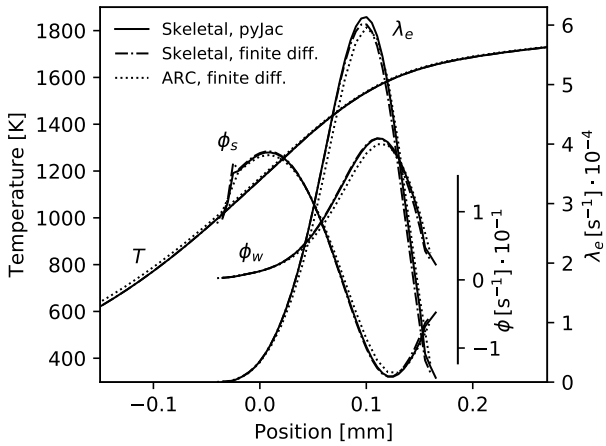


Figure E.28: Application of CEMA to a one-dimensional premixed laminar flame at 1 atm, unburnt temperature $T_u$ and equivalence ratio $\Phi_u$. Multiple configurations are shown: skeletal mechanism and analytical generation of the Jacobian matrix (Skeletal, pyJac), skeletal mechanism and finite difference approximation of the Jacobian matrix (Skeletal, finite diff.), ARC mechanism and finite difference approximation of the Jacobian matrix (ARC, finite diff.). Axial distance is relative to the inflexion point of the temperature profile.